

**TRANSLATIONAL AND CLINICAL RESEARCH**

# Integrated transcriptomic, phenotypic, and functional study reveals tissue-specific immune properties of mesenchymal stromal cells

Cédric Ménard<sup>1,2</sup> | Joëlle Dulong<sup>1,2</sup> | David Roulois<sup>1</sup> | Benjamin Hébraud<sup>3</sup> | Léa Verdière<sup>1</sup> | Céline Pangault<sup>1,4</sup> | Vonick Sibut<sup>1,2</sup> | Isabelle Bezier<sup>1,2</sup> | Nadège Bescher<sup>1,2</sup> | Céline Monvoisin<sup>1</sup> | Mélanie Gadelorge<sup>3</sup> | Nicolas Bertheuil<sup>2,5</sup> | Erwan Flécher<sup>6</sup> | Louis Casteilla<sup>3</sup> | Philippe Collas<sup>7</sup> | Luc Sensebé<sup>3</sup> | Philippe Bourin<sup>8</sup> | Nicolas Espagnolle<sup>3</sup> | Karin Tarte<sup>1,2</sup>

<sup>1</sup>UMR 1236, University of Rennes, INSERM, Etablissement Français du Sang Bretagne, Rennes, France

<sup>2</sup>SITI Laboratory, Etablissement Français du Sang Bretagne, CHU Rennes, Rennes, France

<sup>3</sup>STROMALab, Etablissement Français du Sang-Occitanie (EFS), Inserm 1031, University of Toulouse, National Veterinary School of Toulouse (ENVT), ERL5311 CNRS, Toulouse, France

<sup>4</sup>Pôle Biologie, CHU Rennes, Rennes, France

<sup>5</sup>Department of Plastic Surgery, CHU Rennes, Rennes, France

<sup>6</sup>Department of Thoracic and Cardiac Surgery, CHU Rennes, Rennes, France

<sup>7</sup>Department of Molecular Medicine, Institute of Basic Medical Sciences, Faculty of Medicine, University of Oslo, Oslo, Norway

<sup>8</sup>Cell-Easy, Place Pierre Potier, Toulouse, France

**Correspondence**

Karin Tarte, Pharm D, PhD, INSERM U1236, Faculté de Médecine, 2 Avenue du Pr Léon Bernard, 35043 Rennes, France.  
Email: karin.tarte@univ-rennes1.fr

**Funding information**

Agence Nationale de la Recherche, Grant/Award Numbers: ANR-11-INSB-005, IHU CESTI, ANR-10-IBHU\_0005; CHU Toulouse, Grant/Award Number: Appel d'offre local 2008; Etablissement Français du Sang, Grant/Award Number: APR 2016; Institut National Du Cancer, Grant/Award Number: INCa PLBIO-17-219

**Abstract**

Clinical-grade mesenchymal stromal cells (MSCs) can be expanded from bone marrow and adipose tissue to treat inflammatory diseases and degenerative disorders. However, the influence of their tissue of origin on their functional properties, including their immunosuppressive activity, remains unsolved. In this study, we produced paired bone marrow-derived mesenchymal stromal cell (BM-MSC) and adipose-derived stromal cell (ASC) batches from 14 healthy donors. We then compared them using transcriptomic, phenotypic, and functional analyses and validated our results on purified native MSCs to infer which differences were really endowed by tissue of origin. Cultured MSCs segregated together owing to their tissue of origin based on their gene expression profile analyzed using differential expression and weighted gene coexpression network analysis. This translated into distinct immune-related gene signatures, phenotypes, and functional cell interactions. Importantly, sorted native BM-MSCs and ASCs essentially displayed the same distinctive patterns than their *in vitro*-expanded counterparts. As a whole, ASCs exhibited an immune profile consistent with a stronger inhibition of immune response and a lower immunogenicity, supporting the use of adipose tissue as a valuable source for clinical applications.

**KEYWORDS**

adipose stem cells, bone marrow stromal cells (BMSCs), immunosuppression, immunogenicity, gene expression, cell interactions

## 1 | INTRODUCTION

Mesenchymal stromal cell (MSC) therapy has gained tremendous interest over the past decade, since the seminal proof of concept of its beneficial effect in steroid-resistant graft-versus-host disease.<sup>1,2</sup> MSCs have thereafter been proposed as a valuable innovative approach in a wide array of inflammatory diseases, acute tissue injury syndromes, and chronic degenerative disorders, and more than 900 clinical trials involving MSCs have been registered (<http://www.clinicalTrials.gov>). Nevertheless, the limited evidence of their effectiveness in prospective randomized phase III trials, the lack of defined *in vivo* mechanism of action allowing the design of relevant potency assays and patient monitoring strategies, together with the high cost of regulatory approved cell productions have hampered their development in the clinic.<sup>2,3</sup> Besides heterogeneity of recipients, one possible explanation for the inconsistency in clinical results is the heterogeneity of transplanted MSC batches. In addition to interindividual variability in MSC donors, several critical culture-related parameters affect MSC properties, including culture medium, scale of culture expansion, or cell freezing.<sup>4-6</sup> Accordingly, we have recently shown that replicative senescence associated with industrial-scale expansion of MSCs is associated with a decreased capacity to inhibit T-cell proliferation.<sup>7</sup> Moreover, cryopreservation may behave as an additive detrimental determinant of MSC function and potency.<sup>8</sup>

The tissue source of MSCs was identified early as a major parameter modulating MSC functional properties. The two major sources of clinical-grade MSCs are adult bone marrow (BM) and adipose tissue. Both of them allow the generation of large number of cells expressing the minimal MSC phenotype, that is CD45<sup>neg</sup>CD31<sup>neg</sup>CD14<sup>neg</sup>CD105<sup>pos</sup>CD73<sup>pos</sup>CD90<sup>pos</sup>, and displaying immunosuppressive properties *in vitro*.<sup>4</sup> Cultured adipose-derived stromal cells (ASCs) and bone marrow-derived mesenchymal stromal cells (BM-MSCs) have been proposed to exhibit specific phenotypes, differentiation potentials, secretomes, exosome contents, DNA methylation signatures, as well as transcriptomic, proteomic, and metabolomic profiles.<sup>9-14</sup> However, these findings are not consistent, raising the hypothesis that *in vitro* culture could alter the impact of MSC tissue source. Importantly, MSC clinical efficacy relies on their paracrine activity, including their ability to dampen innate and adaptive immune response.<sup>1</sup> Heterogeneity of MSC production processes but also of immunological assays used to evaluate the impact of MSC tissue sources on their anti-inflammatory and immunosuppressive properties have produced conflicting results.<sup>15,16</sup> Nevertheless, several reports argue for a superiority of ASCs over BM-MSCs to inhibit T-cell activation, in relationship with an increased capacity to produce the immunosuppressive enzyme indoleamine-2,3 dioxygenase (IDO).<sup>17-19</sup>

Strikingly, comparative studies of ASC versus BM-MSC properties almost exclusively analyze MSCs obtained from different donors, sometimes even propagated in different culture conditions, thus precluding any conclusion on the specific role of MSC tissue of origin on the observed variability.<sup>15</sup> In addition, they generally include low numbers of MSC batches, maximizing the influence of interindividual variability. The only large comparison of ASCs and BM-MSCs obtained

### Significance statement

Numerous clinical trials have evaluated the therapeutic potential of mesenchymal stromal cells (MSCs) in degenerative and inflammatory diseases. Whereas their tissue of origin has been proposed as a crucial determinant influencing MSC biological function, the comparison of adipose-derived stromal cell (ASCs) versus bone marrow-derived mesenchymal stromal cells (BM-MSCs) has been essentially performed using MSC batches obtained from different donors, with the confounding influence of interindividual variability. By evaluating transcriptomic, phenotypic, and functional features of paired ASCs and BM-MSCs expanded from the same donors, and analyzing their native purified counterpart, this study highlighted an imprinting of tissue source on MSC immune properties and proposed adipose tissue as a source of MSCs for the treatment of immune-mediated diseases.

from the same donors exclusively focused on *in vitro* immunological functional assays without any evaluation of the molecular mechanisms underlying differences in MSC-driven immunosuppression.<sup>20</sup> Finally, no study has checked whether the observed differences could be detected *in situ* in native MSCs. Overall, the decision to use ASCs versus BM-MSCs is typically motivated by proprietary concerns rather than by validation of their superiority in standardized assays.

The present work was designed to conclude on the biological significance of taking into account MSC tissue source in the design of MSC-based trials. For the first time, we combined transcriptomic, phenotypic, and functional analyses performed on ASCs and BM-MSCs obtained from the same 14 donors, and cultured under identical clinical-grade-like conditions. We identified, using a combination of differential expression, pathway analysis, and weighted gene coexpression network analysis (WGCNA), a specific gene expression profile (GEP) of BM-MSCs versus ASCs with enrichment for niche-related versus immune-related genes. Importantly, we highlighted the same specificities in sorted native BM-MSCs (nBM-MSCs) versus ASCs (nASCs), reinforcing the hypothesis of an imprinting of tissue source on MSC properties. Interestingly, these differences have direct functional consequences on the capacity of MSCs to interact with immune cells. Our results add a new rationale to support the use of adipose tissue as a source of MSCs for the treatment of immune-mediated diseases.

## 2 | MATERIALS AND METHODS

### 2.1 | Cultured MSC production and phenotypic characterization

Healthy donor recruitment followed institutional review board approval and written informed consent process according to the

revised Declaration of Helsinki was obtained. Fourteen donors were enrolled in this study (3 women and 11 men; median age: 36 [21-57] years; body mass index: 16.5-25) and provided BM aspirates (iliac crest) and lipoaspirates (abdominal fat layer). ASCs were obtained after digestion with 0.4 U/mL clinical-grade-NB4 collagenase (Roche Diagnostics, Mannheim, Germany) for 45 minutes at 37°C, filtration, and centrifugation to obtain the stromal vascular fraction (SVF).<sup>21</sup> SVF was seeded at  $4.10^3$  cells per  $\text{cm}^2$  onto CellSTACK closed cell culture chambers (Corning, Lowell, Massachusetts) in  $\alpha$ MEM (Macopharma, Tourcoing, France) supplemented with 10% screened fetal calf serum (Hyclone, Logan, Utah) and 10  $\mu\text{g}/\text{mL}$  ciprofloxacin. Paired BM-MSCs were produced in parallel from unprocessed BM seeded at  $5.10^4$  cells per  $\text{cm}^2$  in the same culture dishes and medium as those used for ASCs. For both MSC types, medium was renewed twice weekly until cells reached confluence (end of passage 0 [P0]). Cells were then detached using trypsin, reseeded at  $1,000/\text{cm}^2$  until near confluence (end of P1) and subsequently harvested and cryopreserved until use. Additional ASC and BM-MSC batches were obtained with the same process from an independent set of healthy donors for validation experiments. For further use, MSCs were thawed, seeded at 1000 cells per  $\text{cm}^2$  and cultured until 80% confluence. All subsequent phenotypic and functional experiments were performed at the end of P2. In particular, MSCs were assessed by flow cytometry for HLA-DR, CD14, CD90, CD73, CD45, CD34, CD105, CD146 (Beckman-Coulter, Villepinte, France), CD31 (eBioscience, Paris, France), and vascular cell adhesion molecule 1 (VCAM-1; Becton-Dickinson, Le Pont de Claix, France) as previously described.<sup>17</sup> Acquisition files were analyzed with Kaluza software (Beckman-Coulter) and data expressed as the ratio of mean fluorescence intensity (rMFI) obtained for each marker and its matched isotypic control antibody.

## 2.2 | Gene expression profiling of cultured MSC

Whole genome gene expression profiling was performed on 14 BM-MSCs and 14 autologous ASCs at the end of P1 using Affymetrix Human Gene 1.0 ST microarrays (Affymetrix, Santa Clara, California) and data were analyzed with R package Limma (v3.32.10). Non-redundant gene datasets were first generated after robust multichip averaging algorithm using GC content normalization by retaining for each gene the probeset with the highest expression. Normalized data were visualized by principal component analysis (PCA) using the R package easy microarray analysis. Pearson correlation with pairwise complete observation was then performed and visualized using heatmap function of the R package made4. Euclidian distance was calculated with the R package stats with ward D2 parameter. Differentially expressed genes were identified based on an adjusted  $P$ -value  $<.05$  (by Benjamini-Hochberg method) and were visualized as a heatmap with the heatmap function in R.

As a secondary method of analysis, we used the WGCNA R package<sup>22</sup> to identify modules of coexpressed genes among the 13 paired MSC batches identified as correctly segregated by the unsupervised

Pearson correlation analysis. For this analysis, we retained the top 25% most variable genes. Expression matrix was log2 transformed and the network was constructed by Pearson correlation considering a soft threshold power ( $\beta$ ) value identified with the function Pick Soft Threshold in order to avoid the selection of an arbitrary cutoff. Then, a topological overlap metric (TOM) matrix was derived from the gene expression matrix and the dissimilarity of TOM was calculated. Hierarchical clustering tree was created and modules were generated by the dynamic tree cut method, with a minimum module size of 100 and a deepSplit of 2. Each module was marked by a color. The module eigengenes were then assigned to each cell type and visualized as a box-plot. To determine if coexpression modules were associated with tissue of origin, we performed a Wilcoxon Signed-Rank test. For the most relevant modules, gene expression was visualized with a heatmap using the heatmap function of the R package. Finally, module gene lists were used for downstream enrichment pathway using the Ingenuity Pathway Analysis software (ingenuity pathway analysis [IPA], QIAGEN Bioinformatics).

For some genes, expression level was also assessed by Q-PCR, as previously described.<sup>17</sup> Briefly, after RNA extraction, gene expression was quantified using Taqman assay-on-demand reagents and an ABI Prism 7000 (Applied Biosystems, Courtaboeuf, France) with the CT calculation method. PCR data were normalized to the geometric mean of two housekeeping genes (*CDKN1B* and *EIF2B1*). Results were further standardized by comparison to gene expression of a pool of five peripheral blood mononuclear cells.

## 2.3 | Analysis of native MSCs

VCAM-1 and HLA-DR expression was assessed on native MSCs after enzymatic digestion of six lipoaspirates and six BM aspirations with the same protocol. Briefly, unprocessed tissue samples were incubated for 45 minutes at 37°C with 200 IU/mL type IV collagenase, 1.6 IU/mL neutral protease (Worthington, Lakewood, New Jersey), and 10 U/mL DNase (Pulmozyme, Genentech, San Francisco, California). Digested tissues were then filtered, washed, and stained with DAPI viability dye and for CD45, CD235a, CD11b (Beckman-Coulter) and CD31 (eBioscience) to gate out hematopoietic and endothelial cells, and CD73, CD146, CD106 (Becton-Dickinson), CD34 (eBioscience), and CD271 (Miltenyi Biotec, Bergisch Gladbach, Germany) to gate stromal cells subsets. nBM-MSCs were gated as  $\text{CD45}/\text{CD235a}/\text{CD11b}/\text{CD31}^{\text{neg}}/\text{CD34}^{\text{neg}}/\text{CD73}^{\text{pos}}/\text{CD271}^{\text{pos}}$  and nASCs as  $\text{CD45}/\text{CD235a}/\text{CD11b}/\text{CD31}^{\text{neg}}/\text{CD34}^{\text{pos}}/\text{CD73}^{\text{pos}}/\text{CD146}^{\text{neg}}$  (see gating strategy in Figure S1) and VCAM-1 and HLA-DR expression was evaluated on both subsets. For sorting of nBM-MSCs, BM mononuclear cells were first collected from enzymatically digested BM using Ficoll gradient and depleted for  $\text{CD45}^{\text{pos}}$  cells using CD45-coupled magnetic beads (Dynabeads, Thermo Fisher Scientific). nBM-MSCs ( $n = 7$ ) and nASCs ( $n = 10$ ) were purified on a FACS Aria II cell sorter (Becton-Dickinson).

Gene expression level in native MSCs was assessed using the Fluidigm BioMark HD system. Briefly, cDNAs were obtained using the

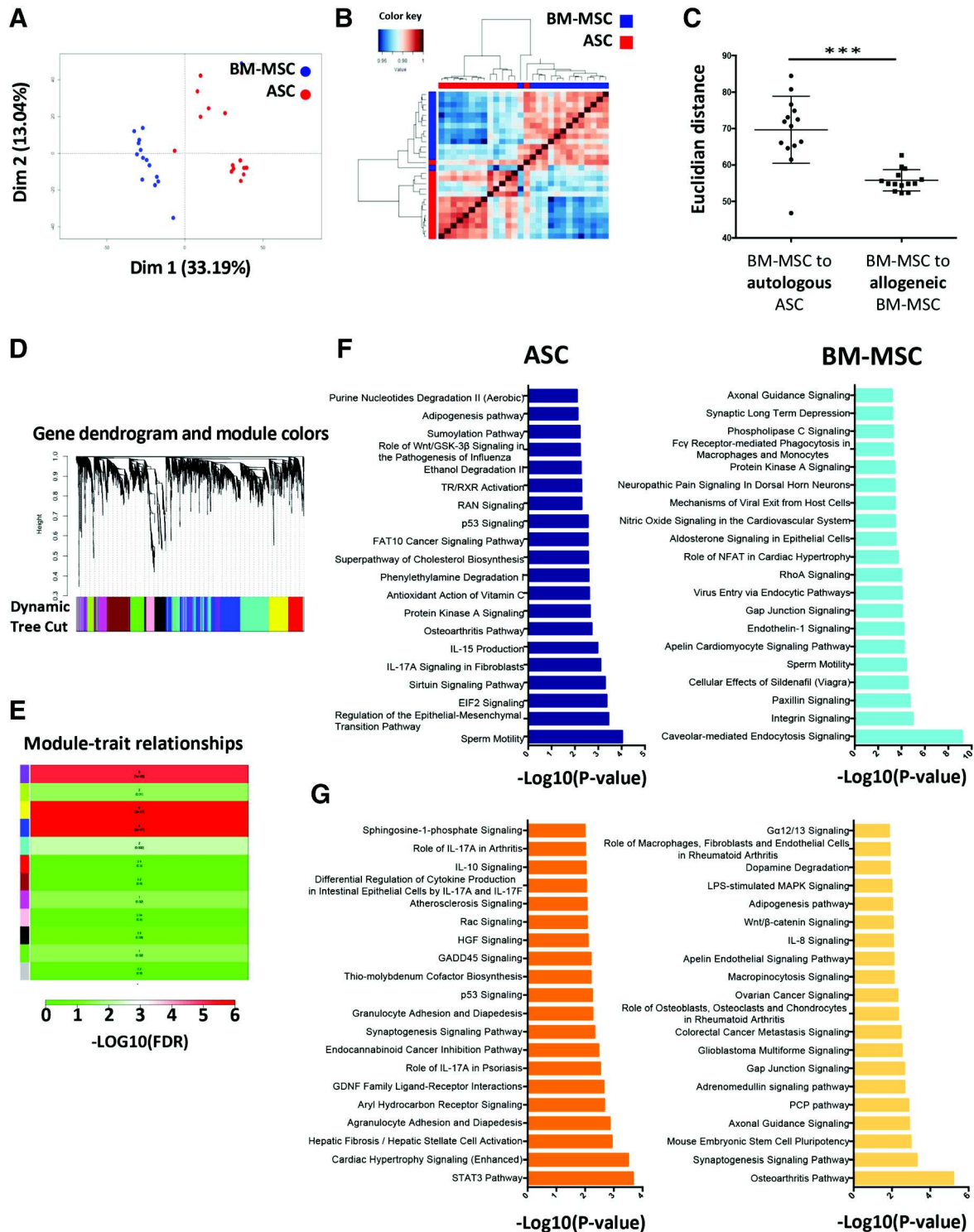


**FIGURE 1** Paired adipose-derived stromal cell (ASC) and bone marrow-derived mesenchymal stromal cell (BM-MSC) transcriptomic analysis reveal tissue-specific signatures. A, Principal component analysis of data resulting from the gene expression profile analysis of 14 paired BM-MSC and ASC samples obtained from the same donors. B, Hierarchical clustering of correlation matrix of paired ASC and BM-MSC gene expression profile using the Pearson's correlation coefficients. C, Euclidian distance between each BM-MSC and its paired ASC versus the mean distance between a given BM-MSC and the geometric mean of the other BM-MSCs; \*\*\* $P < .001$ . D-G, Weighted gene coexpression network analysis. Gene clustering dendrogram and module delimitation based on topological overlap, with different colors representing different coexpression gene modules (D). The relationship between the module eigengenes and the traits (ASC vs. BM-MSC) was then evaluated based on Wilcoxon rank test and was represented as a heatmap color-coded accordingly to the  $-\log_{10}(\text{FDR})$  (E). The genes upregulated in ASCs versus BM-MSCs in the module blue (F) and yellow (G) were analyzed using ingenuity pathway analysis. Shown are the top 20 pathways in ASCs (dark blue and dark orange) and BM-MSCs (light blue and light orange) according to their  $P$ -value

Fluidigm reverse transcription Master Mix and were then preamplified for 18 cycles in the presence of Pre-Amp Master Mix and pooled Taqman assay mix. Gene expression was then measured with the TaqMan Gene Expression Master Mix on a 48.48 Dynamic Array IFC. After quality control check, gene expression was calculated with the CT calculation method and *CDKN1B* and *EIF2B1* as housekeeping genes.

## 2.4 | Impact of MSCs on immune cell apoptosis and adhesion

MSC ability to support survival of immune cells was evaluated as described.<sup>17</sup> Briefly, paired ASCs and BM-MSCs obtained from the

same donors were cocultured with peripheral blood B (1/1 B/MS C ratio), and T cells (10/1 T/MS C ratio) purified using negative selection kits (Miltenyi Biotec, purity >97%). After 3 (B cells) or 7 (T cells) days of coculture, the percentage of apoptotic lymphocytes was assessed by flow cytometry with the Active Caspase-3 Apoptosis kit (Becton-Dickinson) after gating on CD45<sup>POS</sup> events. This allowed for the calculation of the percentage of inhibition of apoptosis with the following formula: (percentage of caspase-3<sup>POS</sup> without MSC – percentage of caspase-3<sup>POS</sup> with MSC)/(percentage of caspase-3<sup>POS</sup> without MSC) × 100.

For adhesion experiments, B cells were stained with 2 μM carboxyfluorescein succinimidyl ester (CFSE; Interchim, Montluçon, France) and plated onto MSC layer for 2 hours as described.<sup>23</sup> After washing in PBS, fluorescence of residual adherent B cells

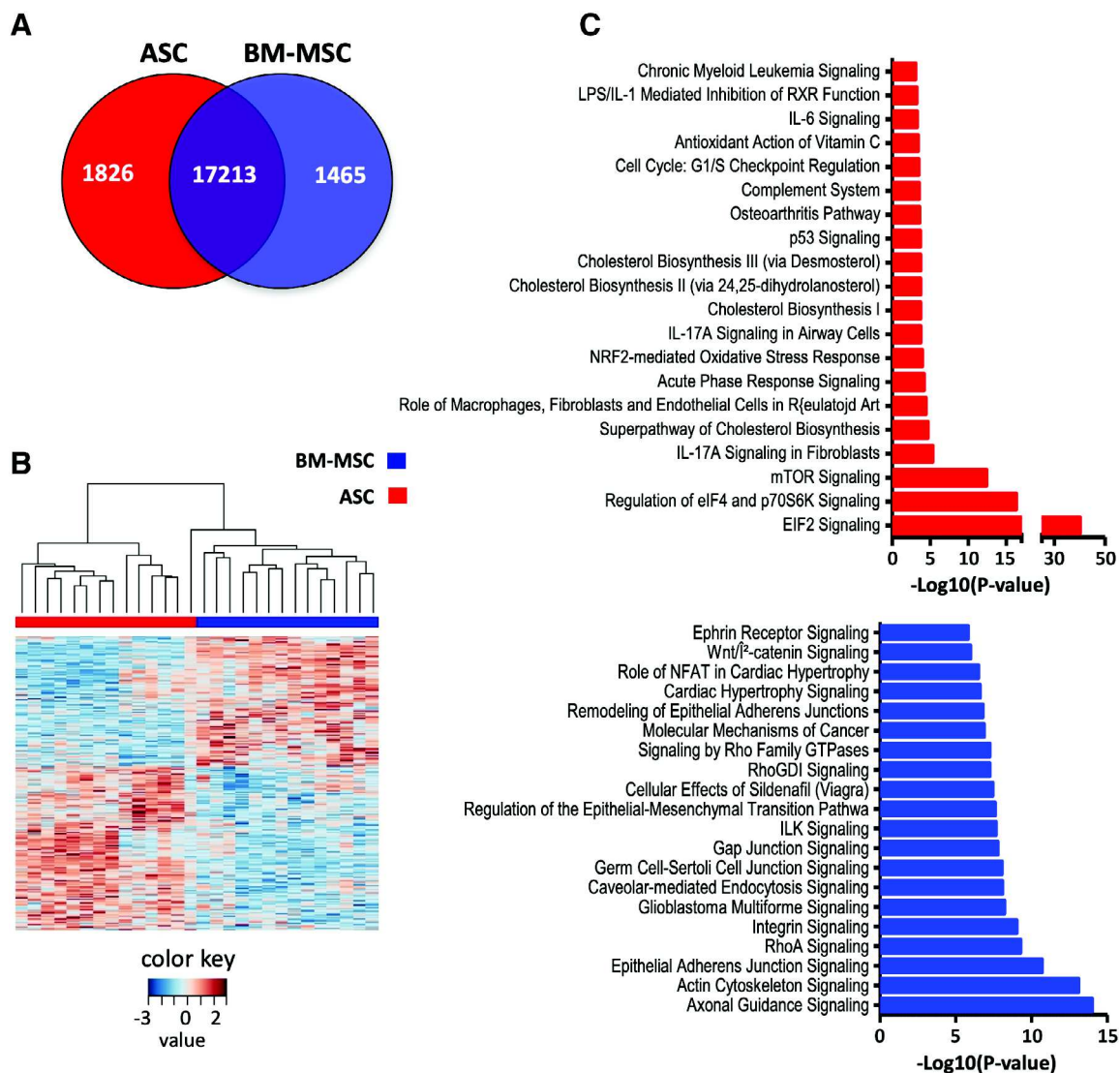


**FIGURE 2** Paired adipose-derived stromal cell (ASC) and bone marrow-derived mesenchymal stromal cell (BM-MSC) differential gene expression pattern highlights tissue-specific functional pathways. A, Venn diagram of the genes differentially expressed between paired BM-MSCs and ASCs ( $n = 14$ ). B, Hierarchical clustering of paired ASCs and BM-MSCs performed on the 3,291 differentially expressed genes. The relative level of gene expression is depicted according to the shown color scale. C, Ingenuity pathway analysis of the upregulated and downregulated genes. Shown are the top 20 pathways in ASCs (top, red bars) and BM-MSCs (bottom, blue bars) according to the  $P$ -value

was recorded on a Varioskan (ThermoFisher) and the percentage of adherent cells was calculated by comparing with the fluorescence of the input. In some experiments, BM-MSCs were transfected with VCAM-1 siRNA (three pooled Stealth iRNA, Life Technologies, Saint-Aubin, France) or a control siRNA (Negative Control Medium GC, Life Technologies) with HiPerfect Transfection Reagent (Qiagen). Briefly, 20,000 BM-MSCs were plated in 96-wells flat-bottomed plates and incubated for 2 days with the transfection mix containing siRNA (50 nM each). Efficient down-regulation of VCAM-1 expression was confirmed by flow cytometry (Figure S2).

## 2.5 | MSC chemoattractive properties

CXCL1 and CXCL16 were quantified in MSC supernatant at the end of P2 by ELISA (R&D Systems, Abington, UK) and expressed as the quantity per million of cultured MSCs.

Migration of neutrophils in response to conditioned MSC supernatants was assessed as previously described<sup>24</sup> with slight modifications. Briefly, peripheral blood neutrophils freshly purified using whole blood CD15 microbeads on an AutoMACS apparatus (Miltenyi Biotech) were added to the upper compartment of Transwell chambers with 5- $\mu$ m pore filters in migration medium (RPMI supplemented with 0.1% human albumin). Lower chambers contained MSC-conditioned supernatants obtained after 3 days of MSC culture in migration medium. The absolute number of viable DAPI<sup>neg</sup>CD66<sup>pos</sup>CD16<sup>pos</sup> neutrophils was quantified in the lower chamber after a 2-hour migration using FlowCount beads by flow cytometry.

## 2.6 | MSC immunosuppressive properties

Inhibition of T and NK cells proliferation was performed as previously described.<sup>17</sup> Briefly, purified peripheral blood T and NK cells were stained with 0.2  $\mu$ M CFSE and activated for 6 days in coculture with MSCs at 10/1 and 1/1 ratios, respectively. T cells were activated with 0.5  $\mu$ g/mL agonistic anti-CD3 and anti-CD28 antibodies (Sanquin, Amsterdam, The Netherlands) whereas NK cells were activated by 100 IU/mL rhIL-2 (Proleukin, Novartis Pharma, Basel, Switzerland). The percentage of proliferating immune cells was quantified by flow cytometry as the proportion of cells having undergone more than one division using the ModFit LT 3.0 software (Verity Software, Topsham, ME). This allowed for the calculation of the percentage of inhibition of proliferation with the following formula: (percentage of proliferation without MSC – percentage of proliferation with MSC)/(percentage of proliferation without MSC) \* 100.

IDO activity was calculated after quantification of tryptophan and kynurenine catabolite by high-performance liquid chromatography using added 3-nitro-L-tyrosine as an internal standard, as previously described.<sup>25</sup> Results were expressed as the kynurenine to tryptophan ratio in the supernatant of MSC primed or not with IFN $\gamma$  (R&D Systems).

## 2.7 | Statistical analysis

Differences between groups were analyzed with Prism software version 5.03 (GraphPad, La Jolla, California) using the Wilcoxon test for matched pairs or the Mann-Whitney nonparametric *U* test for unpaired samples. Differences in dose-response to IFN $\gamma$  stimulation in ASCs versus BM-MSCs were tested with a two-way analysis of variance using Bonferroni's post hoc multiple comparisons tests. In all cases, a cutoff value of *P* < .05 was used to reach statistical significance.

**TABLE 1** Immune-related genes differentially expressed in BM-MSC versus ASC (adjusted *P*-value <.05, |log<sub>2</sub> FC| > 1)

| Upregulated in | Gene symbol     | Log <sub>2</sub> fold change <sup>a</sup> | Adjusted <i>P</i> value |
|----------------|-----------------|---|-------------------------|
| ASC            | <i>PTGS1</i>    | -3.26                                     | 6.82E-08                |
|                | <i>DPP4</i>     | -3.15                                     | 2.30E-05                |
|                | <i>C3</i>       | -3.03                                     | 1.35E-04                |
|                | <i>IL13RA2</i>  | -2.42                                     | 7.92E-04                |
|                | <i>IL1B</i>     | -2.38                                     | 1.91E-05                |
|                | <i>CD55</i>     | -2.37                                     | 3.47E-08                |
|                | <i>TGFBR3</i>   | -2.18                                     | 2.62E-05                |
|                | <i>IL20RB</i>   | -1.97                                     | 4.65E-05                |
|                | <i>CFB</i>      | -1.92                                     | 1.68E-03                |
|                | <i>TNFAIP6</i>  | -1.91                                     | 2.76E-03                |
|                | <i>CXCL2</i>    | -1.81                                     | 2.51E-04                |
|                | <i>ICAM1</i>    | -1.80                                     | 5.98E-06                |
|                | <i>ITGA4</i>    | -1.71                                     | 1.88E-05                |
|                | <i>PTGIS</i>    | -1.69                                     | 6.77E-05                |
|                | <i>C2</i>       | -1.59                                     | 1.38E-04                |
|                | <i>CXCL1</i>    | -1.38                                     | 8.02E-04                |
|                | <i>CFD</i>      | -1.27                                     | 1.19E-02                |
| <i>IL1R1</i>   | -1.19           | 1.53E-03                                  |                         |
| BM-MSC         | <i>VCAM1</i>    | 5.30                                      | 1.32E-05                |
|                | <i>ITGA3</i>    | 2.87                                      | 4.44E-06                |
|                | <i>TGFB2</i>    | 2.33                                      | 1.48E-05                |
|                | <i>ITGA8</i>    | 2.08                                      | 3.81E-04                |
|                | <i>CFH</i>      | 1.97                                      | 1.04E-04                |
|                | <i>ITGB2</i>    | 1.91                                      | 1.54E-04                |
|                | <i>CD74</i>     | 1.82                                      | 1.03E-03                |
|                | <i>STC2</i>     | 1.70                                      | 1.02E-03                |
|                | <i>CXCL16</i>   | 1.38                                      | 3.36E-05                |
|                | <i>ITGA11</i>   | 1.25                                      | 2.21E-04                |
|                | <i>PDCD1LG2</i> | 1.20                                      | 2.06E-03                |
| <i>ITGA10</i>  | 1.14            | 4.90E-04                                  |                         |
| <i>HLA-DRA</i> | 1.05            | 3.32E-02                                  |                         |

Abbreviations: ASC, adipose-derived stromal cell; BM-MSC, bone marrow-derived mesenchymal stromal cell.

<sup>a</sup>Log<sub>2</sub> fold change of expression in BM-MSCs/ASCs.

### 3 | RESULTS

#### 3.1 | ASC and BM-MSC display tissue-specific molecular imprinting

To investigate the net impact of tissue source on cultured MSC properties while minimizing interindividual variability, MSCs were produced in the same culture medium from paired adipose tissue and BM samples collected from 14 healthy individuals. At the end of the first passage (P1), all MSC batches fulfilled the identity criteria including lack of residual hematopoietic and endothelial cells, homogeneous expression of CD90, CD105, and CD73 (Figure S3A). As previously reported CD34 was not expressed on BM-MSCs whereas it could be detected on 17.5% (0.5%-30.7%) of ASCs ( $n = 14$ ). All subsequent experiments were performed at the end of P2 to limit the additional variability associated with large-scale expansion, and closely mimic clinical-grade-MSCs used in successful clinical trials.

We first performed an unbiased transcriptomic analysis using Affymetrix microarrays. PCA including all normalized unique genes (20,507 genes) adequately segregated ASCs from BM-MSCs (Figure 1A). Interestingly, ASC GEP showed a higher heterogeneity than BM-MSC GEP, extending a previous report obtained on a limited number of unpaired allogeneic samples.<sup>12</sup> These data were confirmed by a Pearson correlation analysis in which paired ASCs and BM-MSCs were essentially segregated with a higher level of similarities between BM-MSCs than ASCs (Figure 1B). To better compare the impact of tissue origin versus interindividual variability, we further calculated the Euclidian distance between each BM-MSC and its paired ASC and compared it to the Euclidian distance between each BM-MSC and all the other BM-MSCs (Figure 1C). BM-MSCs were significantly closer to allogeneic BM-MSCs than to autologous ASCs confirming that MSC tissue source impacted MSC transcriptomic heterogeneity to a greater extent than interindividual variability.

We next applied a WGCNA to identify transcriptional modules of coexpressed genes and evaluate whether they were related to MSC

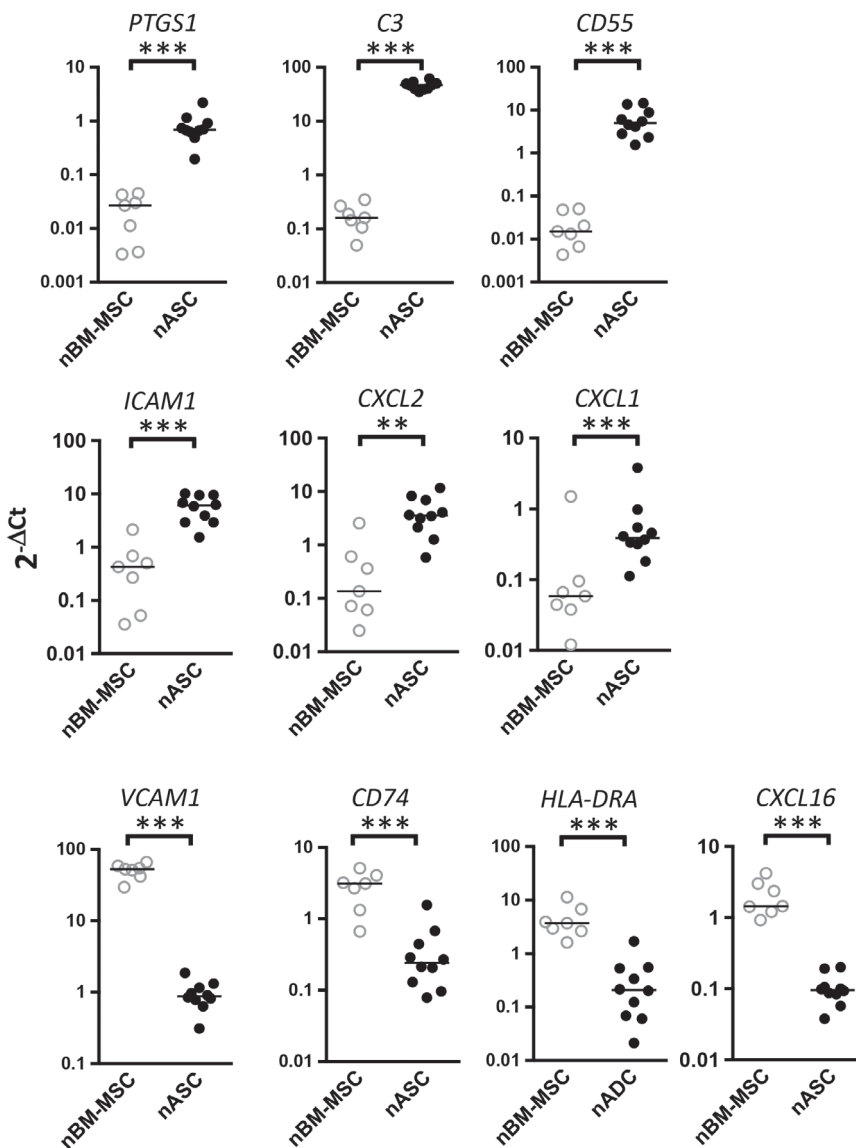


**FIGURE 3** Immune gene expression profile is imprinted by the tissue of origin in mesenchymal stromal cells. Expression of various immune-related genes identified as differentially expressed between paired cultured adipose-derived stromal cells (ASCs) and bone marrow-derived mesenchymal stromal cells (BM-MSCs) using Affymetrix microarrays were assessed by Q-PCR on sorted native ASCs (nASCs,  $n = 10$ ) and native BM-MSCs (nBM-MSCs,  $n = 7$ ). \*\* $P < .01$ ; \*\*\* $P < .001$

tissue source. First, the sample clustering based on Euclidian distance obtained with the WGCNA package (Figure S4A) is in accordance with our previous observations, showing a separation between ASCs and BM-MSCs and a higher heterogeneity of the ASC population. The coexpression network was constructed by Pearson correlation considering a soft-thresholding power  $\beta$  of 8 (Figure S4B). Following dynamic tree cut, the gene clustering dendrogram identified 12 distinct gene modules including the gray module corresponding to unassigned gene (Figure 1D). After the modules were generated, we evaluated their relationship with MSC tissue of origin by using a Wilcoxon Signed-Rank test to determine whether the module eigengenes, defined as the principal component of each module and summarizing the GEP of these modules, were significantly different in ASCs versus BM-MSCs (Figure 1E). Three modules were significantly associated with the MSC tissue source: purple module (264 genes,  $P = 1.346e-06$ ), Yellow module (459 genes,  $P = 1.92e-07$ ), and Blue module ( $P = 1.92e-07$ ; Figure 1E and Figure S4C). Heatmap representation of these gene modules revealed that, conversely to the Purple module, the GEPs of the Yellow and Blue modules perfectly segregated ASCs and BM-MSCs (Figure S4D). In order to draw a functional profile of these two modules, we extracted two genelists per module, one corresponding to the genes overexpressed in ASCs and one to the genes overexpressed in BM-MSCs, and analyzed them with IPA (Figure 1F,G). Interestingly, both Yellow and Blue modules revealed a strong enrichment for immune-related pathways in ASCs. Altogether, our two unsupervised analysis methods clearly indicate that ASCs and BM-MSCs display strongly different transcriptomic profiles that could be functionally relevant for their clinical application.

### 3.2 | Differentially regulated functional pathways in BM-MSCs versus ASCs

Comparison of the GEP of the 28 paired BM-MSCs and ASCs revealed 3,291 differentially expressed unique genes (adjusted  $P$ -value  $< .05$  using Benjamini-Hochberg method, Figure 2A,B), including 208 genes upregulated more than twofold in BM-MSCs and 263 genes upregulated more than twofold in ASCs (log<sub>2</sub> fold change [FC]  $> 1$  or  $< -1$ , Table S1).

As expected, BM-MSC signature was strongly enriched for genes involved in osteogenic and chondrogenic differentiation programs and in the function of osteoblasts and chondrocytes. These include the osteoblastic marker *BGLAP*, the chondrocytic marker *ACAN*, the transcription factors *RUNX3*, *RUNX2*, *DLX5*, *DLX6*, and *SOX9*, the regulator of bone formation *NRP3*, the modulators of pyrophosphate metabolism *ANKH* and *ENPP1*, or *TNFRSF19*, described as a positive regulator of MSC differentiation into osteoblasts while decreasing adipogenesis.<sup>26</sup> Similarly, RhoA signaling, identified as one of the most significant BM-MSC specific pathway using IPA (Figure 2C), has been proposed as a key driver of mechanotransduction in osteoblasts.<sup>27</sup> Canonical Wnt signaling is also essential for osteoblast differentiation and several members of the Wnt pathway were overexpressed in BM-MSCs, whereas ASCs overexpressed some of the main Wnt inhibitors such as

*SFRP1* or *DKK1* (Figure 2C and Table S1). BM-MSCs exhibited a higher capacity to differentiate into chondroblasts in vitro compared with ASCs whereas osteoblastic differentiation was similar (Figure S5A-C). Conversely, ASCs displayed activation of molecular pathways related to cholesterol biosynthesis and *CD36*, the most strongly upregulated ASC gene, is a marker of human adipocyte precursors.<sup>28</sup> Moreover, ASCs displayed a higher capacity to differentiate into adipocytes in vitro (Figure S5D). Altogether, these data definitively confirm that in vitro cultured MSCs retain the main tissue-specific features of their anatomic origin.

Interestingly, cultured BM-MSCs overexpressed genes associated with pericytic BM niche, including a gene set associated with vascular smooth muscle contractility and pericyte identity (*CSPG4*, *ACTA2*,

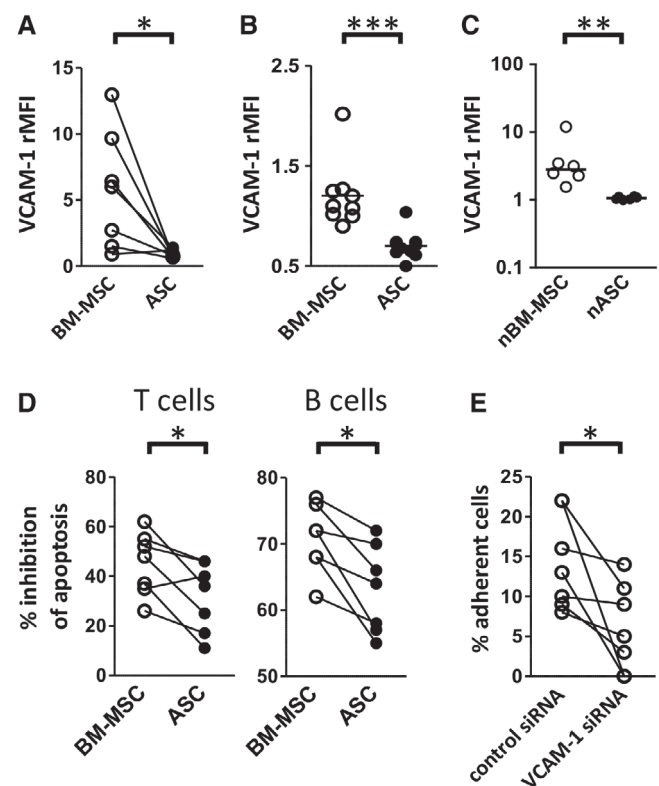


**FIGURE 4** Adipose-derived stromal cells (ASCs) and bone marrow-derived mesenchymal stromal cells (BM-MSCs) differentially mediate immune cell adhesion and survival. A-C, VCAM-1 expression was assessed by flow cytometry on seven paired cultured MSC samples (A), on an independent series of BM-MSCs and ASCs ( $n = 10$  each; B), and on native BM-MSCs (nBM-MSCs) and ASCs (nASCs; C,  $n = 6$  each). D, The ability of MSCs to support immune cell survival was assessed in a coculture assay with resting T and B cells. Survival of CD45<sup>pos</sup> lymphocytes was evaluated by activated caspase-3 staining ( $n = 7$  independent experiments, each time with different paired MSC samples). E, Purified B cells were labeled with CFSE and incubated for 2 hours on BM-MSC confluent cell monolayer. BM-MSCs have been transduced 48 hours before by VCAM-1 targeting siRNA or control siRNA. Adhesion percentage was calculated by comparing the residual fluorescence after adhesion with the fluorescence of the input ( $n = 7$  independent experiments). \* $P < .05$ ; \*\* $P < .01$ ; \*\*\* $P < .001$

MCAM, ITGA7, NOTCH3, MYH9, and MYH11)<sup>29,30</sup> but also extracellular matrix components, including *FNDC1*, *ACAN*, *COL4A1*, *COL4A2*, *HAPLN1*, and *SRGN*; members of the TGF $\beta$  family (*GDF5*, *GDF6*, and *TGFB2*); and numerous integrins (*ITGA3*, *ITGA7*, *ITGA8*, *ITGA11*, and *ITGB2*; Table S1). Overexpression of the pericytic marker CD146/MCAM was confirmed at the protein level (Figure S3B). Conversely, ASC-specific GEP revealed pathways related to immune response and immunosuppression (Fig. 2C). In agreement, numerous immune-related genes were found differentially expressed between ASCs and BM-MSCs (Table 1).

In order to determine whether these differences reflected features of native MSCs or represented a culture artifact, we sorted CD45<sup>neg</sup>CD235a<sup>neg</sup>CD11b<sup>neg</sup>CD31<sup>neg</sup>CD73<sup>pos</sup>CD271<sup>pos</sup> BM mononuclear cells, corresponding to nBM-MSCs, and CD45<sup>neg</sup>CD235a<sup>neg</sup>CD11b<sup>neg</sup>CD31<sup>neg</sup>CD34<sup>pos</sup>CD146<sup>neg</sup> cells from adipose tissue SVF, corresponding to nASCs (Figure S1)<sup>31,32</sup> and analyzed the expression of 10 genes previously found differentially expressed on their cultured counterpart (Table 1). Interestingly, we demonstrated that nASCs significantly overexpressed *PTGS1*, involved in the production of the immunosuppressive molecule PGE2, the complement system members *C3* and *CD55*, the adhesion molecular *ICAM1*, and the CXCR2 ligands *CXCL1* and *CXCL2*. Similarly, nBM-MSCs significantly overexpressed *VCAM1*, antigen presentation molecules *CD74* and *HLA-DRA*, and the chemokine *CXCL16* (Figure 3). These data clearly argue for a strong imprinting of the tissue of origin on the immune properties of cultured MSCs. We thus decided to further examine the

functional consequences of these molecular differences on tissue-specific MSC immune properties.

### 3.3 | BM-MSCs and ASCs differentially trigger immune cell adhesion and recruitment

VCAM-1 was the second most strongly upregulated gene in BM-MSCs. At the protein level VCAM-1 was consistently detected only on BM-MSCs but not on paired ASC counterparts and we further validated this finding on independent MSC batches (Figure 4A, B). Interestingly, nBM-MSCs systematically but variably expressed VCAM-1, whereas nASCs were virtually VCAM-1 negative (Figure 4C). VCAM-1 plays a major role in the anti-apoptotic activity of stromal cells toward immune cells, in particular immature and mature B and T cells expressing the VCAM-1 ligand ITGA4. Moreover, VCAM-1/ITGA4 interaction was proposed years ago as a main determinant of the interaction between pericytes and lymphocytes.<sup>33</sup> We thus wondered whether cultured MSCs could differentially support B and T-cell survival depending on their tissue origin. Strikingly, BM-MSCs protected B and T cells from spontaneous apoptosis in vitro significantly better than their paired ASC counterparts (Figure 4D). In addition, efficient inhibition of VCAM-1 expression in BM-MSCs by siRNA reduced their capacity to trigger B-cell adhesion (Figure 4E).

Apart from adhesion molecules, chemokines also orchestrate the interaction between MSCs and immune cells and both *CXCL1*, *CXCL2*,

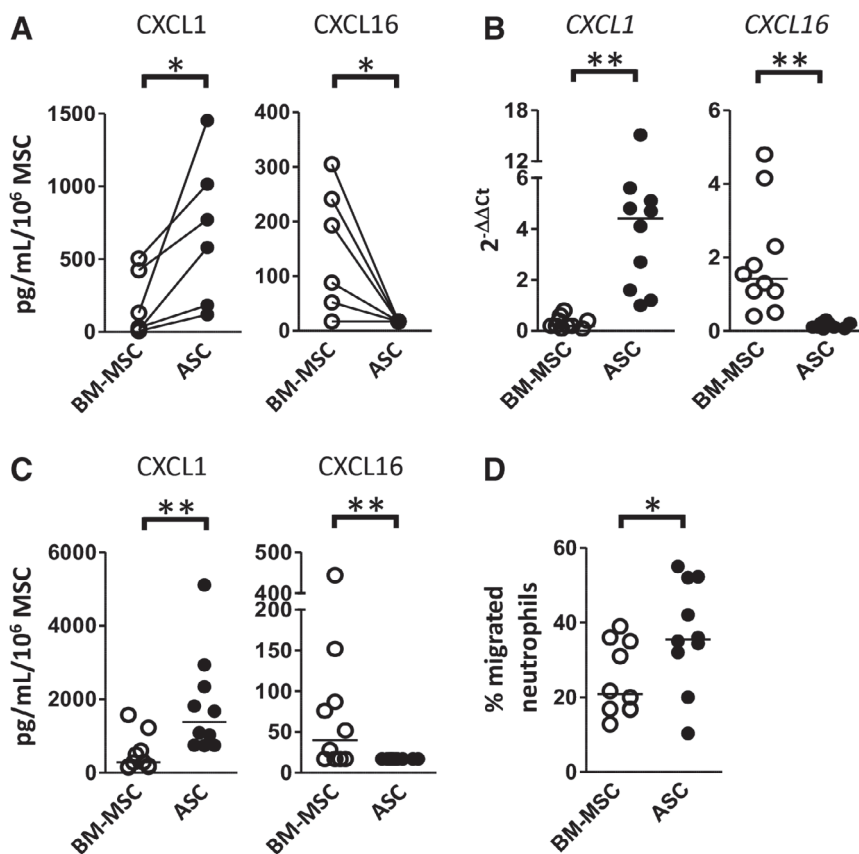
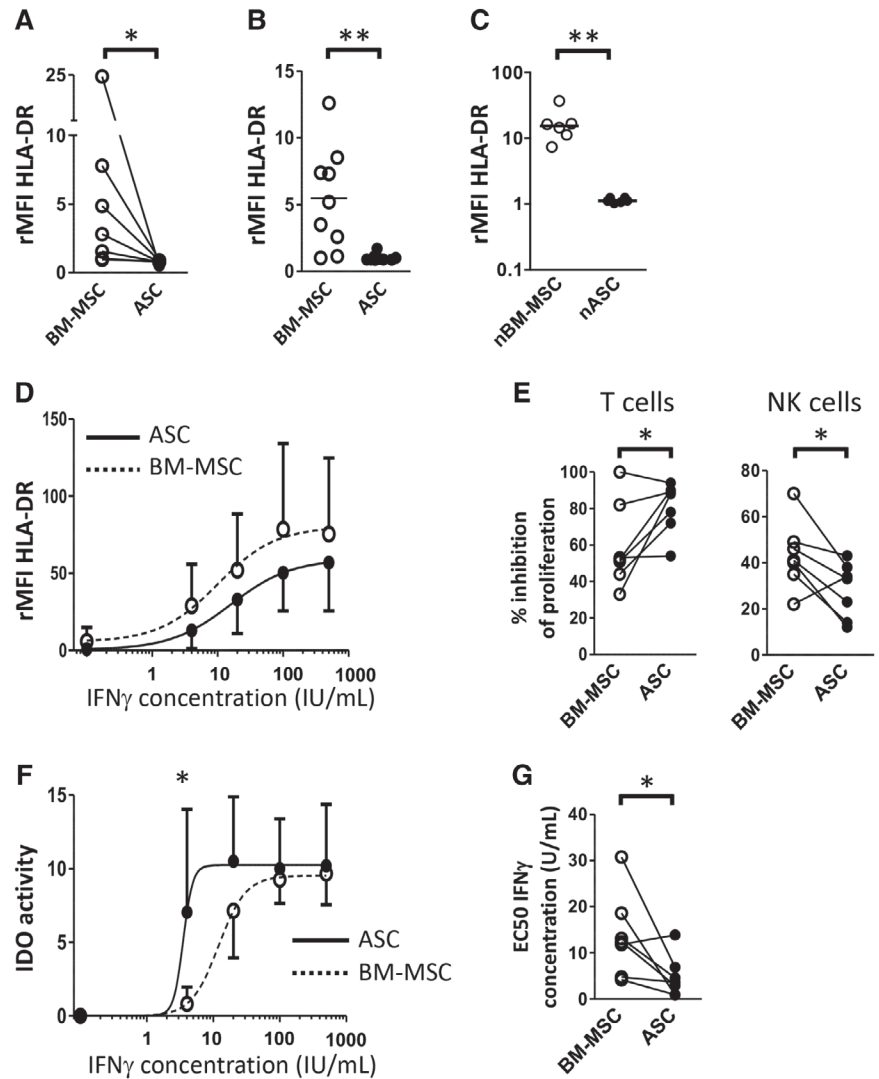


**FIGURE 5** Adipose-derived stromal cells (ASCs) and bone marrow-derived mesenchymal stromal cells (BM-MSCs) have a distinct capacity to attract immune cells. A, CXCL1 and CXCL16 concentrations were quantified in MSC supernatants by ELISA and normalized by the number of cultured MSCs ( $n = 6$  paired MSC samples). B and C, CXCL1 and CXCL16 expression was quantified by Q-PCR (B) and ELISA (C) in an independent series of BM-MSCs and ASCs ( $n = 10$  each). D, Neutrophil migration toward MSC-conditioned medium was quantified by flow cytometry. The percentage of neutrophil migration is calculated as the number of DAPI<sup>neg</sup>CD66b<sup>pos</sup>CD16<sup>pos</sup> viable neutrophils migrating in response to cell supernatant divided by their initial number ( $n = 10$  independent experiments). \* $P < .05$ ; \*\* $P < .01$

**FIGURE 6** Adipose-derived stromal cells (ASCs) and bone marrow-derived mesenchymal stromal cells (BM-MSCs) display different immunomodulatory properties. A-C, HLA-DR expression was assessed by flow cytometry on seven paired cultured MSC samples (A), on an independent series of BM-MSCs and ASCs ( $n = 10$  each; B), and on native BM-MSCs (nBM-MSCs) and ASCs (nASCs; C,  $n = 6$  each). D, Paired MSCs were exposed for 40 hours to increasing concentrations of IFN $\gamma$  before assessment of HLA-DR expression by flow cytometry. Data are represented as median  $\pm$  SD for each IFN $\gamma$  concentration tested ( $n = 7$  paired ASCs and BM-MSCs). E, MSCs were cocultured with CFSE-labeled T and NK cells stimulated with anti-CD3/anti-CD28 or IL-2, respectively. Inhibition of immune cell proliferation was assessed by the CFSE dilution assay after normalization to 100% for the proliferation obtained without MSCs ( $n = 7$  independent experiments with paired MSCs). F, IDO activity was calculated as the ratio of kynurenin and tryptophan concentrations measured in the supernatant of MSCs 40 hours after exposure to increasing doses of IFN $\gamma$ . Data are represented as median  $\pm$  SD for each IFN $\gamma$  concentration ( $n = 7$  paired ASCs and BM-MSCs). G, Half-maximal effective concentrations (EC $_{50}$ ) of IFN $\gamma$  to trigger IDO activity is depicted for each of the seven paired MSC; \*,  $P < .05$ ; \*\*,  $P < .01$ .



and CXCL16 belonged to the most strongly differentially expressed genes between cultured and native ASCs and BM-MSCs (Table 1 and Figure 3). We validated these differences at the protein level on our paired series of cultured BM-MSCs and ASCs as well as on independent MSC batches. As expected, ASCs secreted higher amounts of CXCL1, involved in the recruitment of innate myeloid cells in particular neutrophils, whereas BM-MSCs secreted higher amounts of CXCL16, the ligand for CXCR6-expressing memory T cells and monocytes (Figure 5A-C). Moreover, we could show that, whereas BM-MSCs and ASCs produced the same amount of CXCL8/IL-8, ASCs were significantly more efficient in triggering neutrophil attraction, in agreement with their higher production of CXCL1 and CXCL2, the two other CXCR2 ligands (Figure 5D).

### 3.4 | BM-MSCs and ASCs differentially elicit immune response suppression

The bidirectional crosstalk of infused MSCs with resident immune cells is pivotal for their clinical efficacy. The detection of humoral

alloimmunization in recipients of allogeneic MSCs together with the lack of persistence of infused MSCs demonstrate that MSCs are not immune-privileged.<sup>2</sup> However, protecting MSCs from immune detection and prolonging their life-span in vivo may improve clinical outcome.<sup>34</sup> Cultured and native BM-MSCs were found to overexpress *HLA-DRA* and *CD74*, both involved in antigen presentation to CD4<sup>pos</sup> T cells (Table 1 and Figure 3). We could further confirm surface HLA-DR overexpression on BM-MSCs compared with ASCs in our paired MSC samples, but also on independent cultured MSC batches, and on native MSCs (Figure 6A-C). HLA-DR is induced on MSCs upon exposition to inflammatory cues.<sup>17</sup> We thus tested whether the differential HLA-DR expression between ASCs and BM-MSCs was retained following stimulation by increasing doses of IFN $\gamma$ . Cultured ASCs and BM-MSCs similarly enhanced their HLA-DR expression in response to inflammatory stimuli with a maximum of MHC class II expression at 100 IU/mL of interferon gamma (IFN $\gamma$ ), demonstrating their similar capacity to activate IFN $\gamma$ -dependent signaling pathway. As a consequence, the level of expression of HLA-DR remained lower on inflamed ASC than on inflamed BM-MSC (Figure 6D). These data suggested that ASCs could better escape to recognition by CD4<sup>pos</sup> T

cells. In addition, their higher expression of the cell-surface complement inhibitor *CD55* (Table 1), previously shown to crucially regulate MSC sensitivity to complement-dependent cytotoxicity,<sup>35</sup> could favor their escape from initial immune attack *in vivo*.

We then used our previously established standardized tools to compare the capacity of paired ASCs and BM-MSCs to inhibit activated T-cell and NK-cell proliferation *in vitro*.<sup>17</sup> Strikingly, ASCs decreased significantly better T-cell proliferation and BM-MSCs significantly better NK cell proliferation (Figure 6E). We and others have shown that IDO activity is the main mechanism supporting the capacity of human MSCs to suppress T cells, unlike NK cells.<sup>17</sup> IDO is not expressed by resting MSCs but is induced by IFN $\gamma$  produced by activated T and NK cells. We thus assessed IDO activity in ASCs and BM-MSCs licensed with increasing doses of IFN $\gamma$ . We showed that ASCs required significantly less IFN $\gamma$  to reach the maximum IDO activity than BM-MSCs (Figure 5F,G). Thus, whereas ASCs and BM-MSCs have the same intrinsic capacity to respond to IFN $\gamma$  signaling, as highlighted by parallel curves of HLA-DR induction, ASCs express higher functional immunosuppressive enzyme IDO in response to a low dose of IFN $\gamma$ .

## 4 | DISCUSSION

Tissue origin has been proposed for a long-time as a potential determinant of clinical-grade MSC clinical efficacy. However, how intrinsic disparities between BM-MSCs and ASCs could be related to their capacity to interact with immune effectors and modulate immune response has not been extensively explored. In the present study, we demonstrated for the first time on a large series of ASCs and BM-MSCs obtained from the same donors and on purified nASCs and nBM-MSCs the strong impact of tissue origin on MSC properties. Moreover, we pinpointed that ASCs could be an interesting alternative to BM-MSCs for therapeutic applications considering their huge expression of anti-inflammatory and immunosuppressive molecules.

First, ASCs endorsed stronger IDO activity in response to low dose IFN- $\gamma$  stimulation, thereafter inhibiting more efficiently T-cell proliferation. Interestingly, ASCs display a higher proliferative capacity *in vitro* and enter senescence at a later time point compared with BM-MSCs thus delaying the risk of proteasomal degradation of IDO that characterizes senescent MSCs.<sup>7</sup> In agreement, the clinical impact of culture expansion has been validated by the demonstration that late-passage MSCs were less effective than early-passage MSCs to control acute graft-versus-host-disease.<sup>36</sup> Of note, the IDO<sup>hi</sup> phenotype of ASCs could be further reinforced by the direct contact with innate myeloid cells, a key step in tissue repair and regeneration. In fact, the interplay between MSCs and inflammatory macrophages was recently shown to trigger IDO expression and activity in MSCs in a CD54-dependent manner<sup>37</sup> and ASCs overexpressed CD54/ICAM-1 compared with BM-MSCs.

Second, resting ASCs overexpressed tumor necrosis factor-stimulated gene 6 (TSG-6), involved in the early inhibition of neutrophil and macrophage activity at sites of inflammation. Kynurenic acid, a tryptophan metabolite generated by IDO, was recently shown to enhance TSG-6 expression through the activation of aryl hydrocarbon

receptor (AhR), which binds to *TNFAIP6* promoter.<sup>38</sup> This amplification loop between the two main MSC immunosuppressive mediators could contribute to the higher TSG-6 expression in ASCs primed by inflammatory stimuli. TSG-6 was proposed to directly impact the NF- $\kappa$ B dependent activation of macrophages by TLR ligands<sup>39</sup> whereas IDO has been implicated in the differentiation of monocytes into IL-10-secreting immunosuppressive macrophages.<sup>40</sup> It is thus tempting to speculate that, besides their strong capacity to inhibit T cells and their interest for the treatment of T-cell-mediated immune disorders, ASCs would be particularly effective in modulating the inflammatory response mediated by macrophages. In addition, we revealed that ASCs recruited more efficiently neutrophils than BM-MSCs, whereas they overexpressed TSG-6, recently identified as a CXCL8-binding protein inhibiting neutrophil transendothelial migration and chemotaxis.<sup>41</sup> However, TSG-6 does not bind to CXCL1/CXCL2, both upregulated in ASCs, and has no effect on CXCL1-mediated neutrophil transmigration.

Finally, ASCs were virtually HLA-DR<sup>neg</sup> and retained a lower HLA-DR expression under inflammatory stimuli compared with BM-MSCs. This property could be clinically relevant in relationship with the increasing use of MSCs in allogeneic setting. However, a comparison of alloimmunization rates in homogeneous patients receiving ASCs versus BM-MSCs is currently lacking to conclude on the lower immunogenicity of ASCs. Interestingly, we highlighted for the first time an upregulation of components of the complement activation cascade in ASC transcriptomic profile. Complement components were recently identified as promoters of immunological tolerance through their capacity to promote development of myeloid-derived suppressor cells (MDSCs).<sup>42</sup> In particular, liver stromal cells, like ASCs, produce C3, Factor B, and Factor D resulting in the formation of activation products iC3b and C3d that trigger dendritic cell differentiation into MDSCs.<sup>43</sup> The role of complement activation in the immunosuppressive activity of MSCs deserves further investigations. Importantly, it has to be noted that ASCs were conversely less potent than BM-MSCs at preventing NK cell proliferation, in agreement with the lack of reversion of MSC-dependent NK-suppressive activity by IDO inhibitors.<sup>44,45</sup> In addition, BM-MSCs overexpressed PD-L1/CD274 and stanniocalcin-2 (STC2), two suppressive molecules affecting CD8<sup>pos</sup> T-cell activation and synthesis of inflammatory cytokines.<sup>44,45</sup>

Of note, we restrained our study to lean MSC donors to avoid any confounding impact of obesity. In fact, cultured ASCs obtained from obese patients were reported to display reduced immunosuppressive activities in classical *in vitro* assays.<sup>46</sup> Moreover, a recent study revealed that obesity differentially impacts the molecular phenotype, the differentiation/commitment potential, and the metabolic profile of BM-MSCs versus ASCs, thus potentially variably affecting their immune properties.<sup>47,48</sup> Finally, obese BM is characterized by an altered hematopoiesis whereas obese adipose tissue is characterized by an accumulation of innate and adaptive pro-inflammatory immune cells, all parameters that could indirectly impact MSC immune properties. A detailed analysis of paired ASCs/BM-MSCs obtained from overweighted/obese patients is thus required to conclude on the specific impact of obesity on their respective immune functions.

The mechanisms underlying the higher IDO activity in ASCs in response to IFN $\gamma$  are still unclear whereas IDO expression and activity has been reproducibly correlated with the capacity of human MSCs to inhibit T-cell proliferation.<sup>17,40,49</sup> BM-MSCs and ASCs expressed IFN $\gamma$  receptor at the same level (data not shown) and similarly upregulated HLA-DR in response to IFN $\gamma$  stimulation, indicating a functional IFN $\gamma$  signaling pathway. Of note IDO mRNA level was also reduced in primed BM-MSCs compared with primed ASCs (data not shown) suggesting a regulation at the transcriptional level. Recently, histone modifications at *IDO1* promoter region were shown to be induced upon inflammatory cytokine treatment of BM-MSCs, with a loss of H3K9me3 repressive mark and a gain of permissive acH3K9 mark.<sup>50</sup> Methylation of the *IDO1* promoter was also proposed as an additional level of regulation of IDO expression in breast cancer cells.<sup>51</sup> A deeper evaluation of epigenetic regulation of *IDO1* in ASCs versus BM-MSCs should shed new light on the regulation of this immunosuppressive mediator in the two cell subsets.

Importantly, we revealed for the first time, using purified nASCs and nBM-MSCs, that the differential immune profile of in vitro-expanded MSCs obtained from BM and adipose tissue is essentially imprinted by their tissue of origin. Interestingly, murine ASCs were proposed to be the precursors of lymphoid stromal cells that regulate immune cell recruitment and guided trafficking inside secondary lymphoid organs and ensure antigen delivery and B-cell activation and selection.<sup>52</sup> We highlighted here a lymphoid stroma signature, including *LTBR*, the NF- $\kappa$ B family members *IRAK1*, *IRAK3*, and *TRAF3IP2*; *IL4R*, *IL13RA2*, *CLU*, and *CSTC* in cultured human ASCs compared with BM-MSCs further confirming the relationship between in vitro-expanded ASCs and their native counterpart and suggested that these cells are prone to interact with immune cells in vivo.

## 5 | CONCLUSION

Besides variations in culture procedures, immunological properties of ASCs and BM-MSCs are strongly related to their tissue of origin and in vitro-expanded MSCs retain the main features of their native counterpart. In particular, ASCs overexpress several molecules associated with an increased capacity to modulate immune cells and have a transcriptomic and phenotypic profile consistent with a lower immunogenicity. This study paves the way for a better definition of potency assays based on a simultaneous evaluation of molecular and cellular targets. In addition, it could also be helpful to evaluate how MSC modifications or reprogramming could enhance their clinical potency.

## ACKNOWLEDGMENTS

We thank Jérôme Moreaux and Alboukadel Kassambara for helpful discussions. This work was supported by grants from the CHU de Toulouse (Appel d'offre local 2008), the Etablissement Français du Sang (APR 2016), the Infrastructure program EcellFRANCE (ANR-11-INB-005), the European Center for Transplantation Sciences and Immunotherapy (IHU CESTI, ANR-10-IHUB-0005), the French National Cancer Institute (INCa PLBIO-17-219). L.V. is a recipient of a fellowship from the Labex IGO (ANR-11-LABX-0016-01) and the Région Bretagne.

## AUTHOR CONTRIBUTIONS

C. Ménard: collection and assembly of data, data analysis and interpretation, manuscript writing, final approval; J.D., L.V., I.B., N. Bescher, M.G., P.C., C. Monvoisin: collection and assembly of data; D.R.: data analysis and interpretation, manuscript writing; C.P., V.S.: data analysis and interpretation; N. Bertheuil, E.F.: provision of study material or donors; B.H.: collection and assembly of data, provision of study material or donors; L.S.: contribution to data interpretation and manuscript writing; L.C., P.B., N.E.: conception and design of the study; K.T.: conception and design of the study, financial support, data analysis and interpretation, manuscript writing and final approval.

## CONFLICT OF INTEREST

The authors indicated no potential conflicts of interest.

## DATA AVAILABILITY STATEMENT

Data are available via the NCBI Gene Expression Omnibus (<https://www.ncbi.nlm.nih.gov/geo/>; accession number GSE122778).

## ORCID

Karin Tarte  <https://orcid.org/0000-0002-6809-917X>

## REFERENCES

- Shi Y, Wang Y, Li Q, et al. Immunoregulatory mechanisms of mesenchymal stem and stromal cells in inflammatory diseases. *Nat Rev Nephrol* 2018;14:493-507.
- Galipeau J, Sensebé L. Mesenchymal stromal cells: clinical challenges and therapeutic opportunities. *Cell Stem Cell* 2018;22:824-833.
- Galipeau J. The mesenchymal stromal cells dilemma—does a negative phase III trial of random donor mesenchymal stromal cells in steroid-resistant graft-versus-host disease represent a death knell or a bump in the road? *Cytotherapy* 2013;15:2-8.
- Sensebé L, Bourin P, Tarte K. Good manufacturing practices production of mesenchymal stem/stromal cells. *Hum Gene Ther* 2011;22:19-26.
- Mendicino M, Bailey AM, Wonnacott K, et al. MSC-based product characterization for clinical trials: an FDA perspective. *Cell Stem Cell* 2014;14:141-145.
- Moll G, Alm JJ, Davies LC, et al. Do cryopreserved mesenchymal stromal cells display impaired immunomodulatory and therapeutic properties? *STEM CELLS* 2014;32:2430-2442.
- Loisel S, Dulong J, Ménard C, et al. Brief report: proteasomal indoleamine 2,3-dioxygenase degradation reduces the immunosuppressive potential of clinical grade-mesenchymal stromal cells undergoing replicative senescence. *STEM CELLS* 2017;35:1431-1436.
- Chinnadurai R, Copland IB, Garcia MA, et al. Cryopreserved mesenchymal stromal cells are susceptible to T-cell mediated apoptosis which is partly rescued by IFN $\gamma$  licensing. *STEM CELLS* 2016;34:2429-2442.
- Cho K-A, Park M, Kim Y-H, et al. RNA sequencing reveals a transcriptomic portrait of human mesenchymal stem cells from bone marrow, adipose tissue, and palatine tonsils. *Sci Rep* 2017;7:17114.
- de Almeida DC, Ferreira MRP, Franzen J, et al. Epigenetic classification of human mesenchymal stromal cells. *Stem Cell Rep* 2016;6:168-175.
- Jansen BJH, Gilissen C, Roelofs H, et al. Functional differences between mesenchymal stem cell populations are reflected by their transcriptome. *Stem Cells Dev* 2010;19:481-490.

12. Torensma R, Prins H-J, Schrama E, et al. The impact of cell source, culture methodology, culture location, and individual donors on gene expression profiles of bone marrow-derived and adipose-derived stromal cells. *Stem Cells Dev* 2013;22:1086-1096.
13. Lee SJ, Yi T, Ahn SH, et al. Comparative study on metabolite level in tissue-specific human mesenchymal stem cells by an ultra-performance liquid chromatography quadrupole time of flight mass spectrometry. *Anal Chim Acta* 2018;1024:112-122.
14. Reinisch A, Etchart N, Thomas D, et al. Epigenetic and in vivo comparison of diverse MSC sources reveals an endochondral signature for human hematopoietic niche formation. *Blood* 2015;125:249-260.
15. Mattar P, Bieback K. Comparing the immunomodulatory properties of bone marrow, adipose tissue, and birth-associated tissue mesenchymal stromal cells. *Front Immunol* 2015;6:560.
16. Ménard C, Tarte K. Immunoregulatory properties of clinical grade mesenchymal stromal cells: evidence, uncertainties, and clinical application. *Stem Cell Res Ther* 2013;4:64.
17. Ménard C, Pacelli L, Bassi G, et al. Clinical-grade mesenchymal stromal cells produced under various good manufacturing practice processes differ in their immunomodulatory properties: standardization of immune quality controls. *Stem Cells Dev* 2013;22:1789-1801.
18. Melief SM, Zwaginga JJ, Fibbe WE, et al. Adipose tissue-derived multipotent stromal cells have a higher immunomodulatory capacity than their bone marrow-derived counterparts. *STEM CELLS Translational Medicine* 2013;2:455-463.
19. Ribeiro A, Laranjeira P, Mendes S, et al. Mesenchymal stem cells from umbilical cord matrix, adipose tissue and bone marrow exhibit different capability to suppress peripheral blood B, natural killer and T cells. *Stem Cell Res Ther* 2013;4:125.
20. Valencia J, Blanco B, Yáñez R, et al. Comparative analysis of the immunomodulatory capacities of human bone marrow- and adipose tissue-derived mesenchymal stromal cells from the same donor. *Cytotherapy* 2016;18:1297-1311.
21. Bourin P, Peyrafitte J-A, Fleury-Cappellesso S. A first approach for the production of human adipose tissue-derived stromal cells for therapeutic use. *Methods Mol Biol* 2011;702:331-343.
22. Langfelder P, Horvath S. WGCNA: an R package for weighted correlation network analysis. *BMC Bioinf* 2008;9:559.
23. Pandey S, Mourcin F, Marchand T, et al. IL-4/CXCL12 loop is a key regulator of lymphoid stroma function in follicular lymphoma. *Blood* 2017;129:2507-2518.
24. Grégoire M, Guilloton F, Pangault C, et al. Neutrophils trigger a NF- $\kappa$ B dependent polarization of tumor-supportive stromal cells in germinal center B-cell lymphomas. *Oncotarget* 2015;6:16471-16487.
25. Tattevin P, Monnier D, Tribut O, et al. Enhanced indoleamine 2,3-dioxygenase activity in patients with severe sepsis and septic shock. *J Infect Dis* 2010;201:956-966.
26. Qiu W, Hu Y, Andersen TE, et al. Tumor necrosis factor receptor superfamily member 19 (TNFRSF19) regulates differentiation fate of human mesenchymal (stromal) stem cells through canonical Wnt signaling and C/EBP. *J Biol Chem* 2010;285:14438-14449.
27. Nobis M, Herrmann D, Warren SC, et al. A RhoA-FRET biosensor mouse for intravital imaging in normal tissue homeostasis and disease contexts. *Cell Rep* 2017;21:274-288.
28. Gao H, Volat F, Sandhow L, et al. CD36 is a marker of human adipocyte progenitors with pronounced adipogenic and triglyceride accumulation potential. *STEM CELLS* 2017;35:1799-1814.
29. Armulik A, Genové G, Betsholtz C. Pericytes: developmental, physiological, and pathological perspectives, problems, and promises. *Dev Cell* 2011;21:193-215.
30. Astarita J, Lukacs-Kornek V, Tayalia P, et al. Transcriptional profiling of stroma from inflamed and resting lymph nodes defines immunological hallmarks. *Nat Immunol* 2012;13:499-510.
31. Li H, Ghazanfari R, Zacharaki D, et al. Isolation and characterization of primary bone marrow mesenchymal stromal cells. *Ann N Y Acad Sci* 2016;1370:109-118.
32. Maumus M, Peyrafitte J-A, D'Angelo R, et al. Native human adipose stromal cells: localization, morphology and phenotype. *Int J Obes* 2011;35:1141-1153.
33. Navarro R, Compte M, Álvarez-Vallina L, et al. Immune regulation by pericytes: modulating innate and adaptive immunity. *Front Immunol* 2016;7:480.
34. Ankrum JA, Ong JF, Karp JM. Mesenchymal stem cells: immune evasive, not immune privileged. *Nat Biotechnol* 2014;32:252-260.
35. Li Y, Lin F. Mesenchymal stem cells are injured by complement after their contact with serum. *Blood* 2012;120:3436-3443.
36. von L B, Sundberg B, Lönnies L, et al. Long-term complications, immunologic effects, and role of passage for outcome in mesenchymal stromal cell therapy. *Biol Blood Marrow Transplant* 2012;18:557-564.
37. Espagnolle N, Balguerie A, Arnaud E, et al. CD54-mediated interaction with pro-inflammatory macrophages increases the immunosuppressive function of human mesenchymal stromal cells. *Stem Cell Rep* 2017;8:961-976.
38. Wang G, Cao K, Liu K, et al. Kynurenic acid, an IDO metabolite, controls TSG-6-mediated immunosuppression of human mesenchymal stem cells. *Cell Death Differ* 2018;25:1209-1223.
39. Choi H, Lee RH, Bazhanov N, et al. Anti-inflammatory protein TSG-6 secreted by activated MSCs attenuates zymosan-induced mouse peritonitis by decreasing TLR2/NF- $\kappa$ B signaling in resident macrophages. *Blood* 2011;118:330-338.
40. François M, Romieu-Mourez R, Li M, et al. Human MSC suppression correlates with cytokine induction of indoleamine 2,3-dioxygenase and bystander M2 macrophage differentiation. *Mol Ther* 2012;20:187-195.
41. Dyer DP, Thomson JM, Hermant A, et al. TSG-6 inhibits neutrophil migration via direct interaction with the chemokine CXCL8. *J Immunol* 2014;192:2177-2185.
42. Luque A, Serrano I, Aran JM. Complement components as promoters of immunological tolerance in dendritic cells. *Semin Cell Dev Biol* 2019;85:143-152.
43. Hsieh C-C, Chou H-S, Yang H-R, et al. The role of complement component 3 (C3) in differentiation of myeloid-derived suppressor cells. *Blood* 2013;121:1760-1768.
44. Davies LC, Heldring N, Kadri N, et al. Mesenchymal stromal cell secretion of programmed death-1 ligands regulates T cell mediated immunosuppression. *STEM CELLS* 2017;35:766-776.
45. Chen X, Liu Q, Huang W, et al. Stanniocalcin-2 contributes to mesenchymal stromal cells attenuating murine contact hypersensitivity mainly via reducing CD8+ Tc1 cells. *Cell Death Dis* 2018;9:548.
46. Serena C, Keiran N, Ceperuelo-Mallafre V, et al. Obesity and type 2 diabetes alters the immune properties of human adipose derived stem cells. *STEM CELLS* 2016;34:2559-2573.
47. Tencerova M, Frost M, Figeac F, et al. Obesity-associated hypermetabolism and accelerated senescence of bone marrow stromal stem cells suggest a potential mechanism for bone fragility. *Cell Rep* 2019;27:2050.e2056-2062.e2056.

48. Louwen F, Ritter A, Kreis NN, et al. Insight into the development of obesity: functional alterations of adipose-derived mesenchymal stem cells. *Obes Rev* 2018;19:888-904.
49. Chinnadurai R, Rajan D, Qayed M, et al. Potency analysis of mesenchymal stromal cells using a combinatorial assay matrix approach. *Cell Rep* 2018;22:2504-2517.
50. Rovira Gonzalez YI, Lynch PJ, Thompson EE, et al. In vitro cytokine licensing induces persistent permissive chromatin at the Indoleamine 2,3-dioxygenase promoter. *Cytotherapy* 2016;18:1114-1128.
51. Dewi DL, Mohapatra SR, Blanco Cabañes S, et al. Suppression of indoleamine-2,3-dioxygenase 1 expression by promoter hypermethylation in ER-positive breast cancer. *Oncoimmunology* 2017;6:e1274477.
52. Bénézéch C, Mader E, Desanti G, et al. Lymphotoxin-beta receptor signaling through NF-kappa B2-RelB pathway reprograms adipocyte precursors as lymph node stromal cells. *Immunity* 2012;37:721-734.

#### SUPPORTING INFORMATION

Additional supporting information may be found online in the Supporting Information section.

**How to cite this article:** Ménard C, Dulong J, Roulois D, et al. Integrated transcriptomic, phenotypic, and functional study reveals tissue-specific immune properties of mesenchymal stromal cells. *Stem Cells*. 2020;38:146–159. <https://doi.org/10.1002/stem.3077>